Graphical Abstract

Thermal design on non-isothermal microfluidic channel for measuring thermophoresis

Namkyu Lee,Simone Wiegand

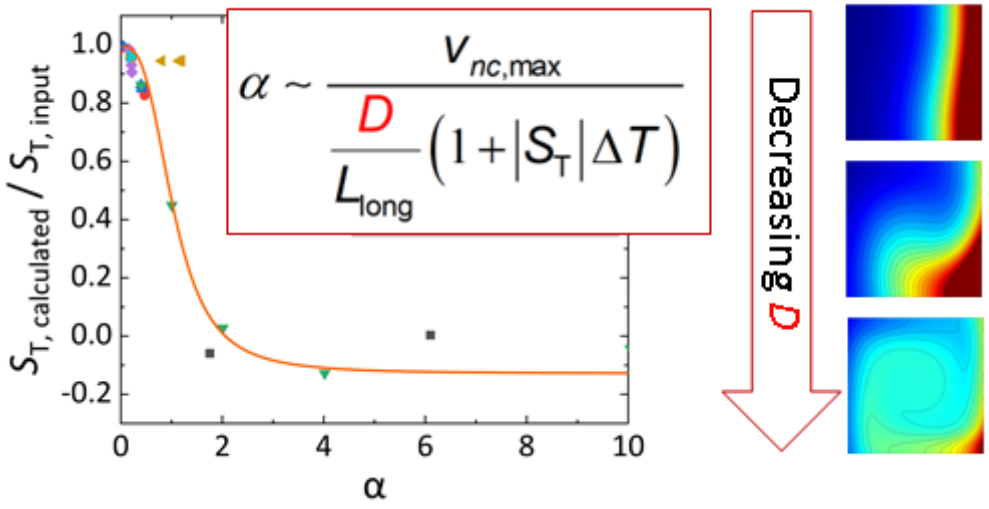

Highlights

Thermal design on non-isothermal microfluidic channel for measuring thermophoresis

Namkyu Lee,Simone Wiegand

- The thermal design of thermophoretic cells is analyzed by considering fluid dynamics, heat transfer, and mass transfer.
- A figure of merit is suggested for thermal design on non-isothermal microfluidic channels employing natural convection and thermophoresis.
- The unity of the figure of merit distinguishes diffusion- and convection-dominant fields in the thermophoretic cell.
- Figure of merit provides the criterion for reliable measurement of the Soret coefficient in the thermophoretic cell.

Thermal design on non-isothermal microfluidic channel for measuring thermophoresis

Namkyu Lee[a,b,*], Simone Wiegand[b,c,*]

[a]Departement of Mechanical Engineering, Yonsei University, 03722, Korea
[b]IBI-4, Forschungzentrum Jülich, 52428, Germany
[c]Universität zu Köln, 50939, Germany

ARTICLE INFO

Keywords:
Thermal design, Thermophoreis, Soret coefficient, Microfluidics, Natural convection

ABSTRACT

Thermophoresis describes mass transport in a non-isothermal temperature field and thus provides a fundamental understanding of the behavior of colloidal particles. Various methods have been proposed for measuring the Soret coefficient, a representative value of thermophoresis. In particular, microscopic channels are an emerging method as they shorten the equilibrium time and allow direct observation of the particles. However, little emphasis has been placed on the simultaneous consideration of fluid dynamics, heat transfer, and mass transfer characteristics within the microfluidic channel, despite the simultaneous presence of natural convection and thermodiffusion phenomena. In this study, we present a novel approach to address this gap by introducing a *figure of merit*, which incorporates essential parameters to accurately characterize a specific cell configuration. This *figure of merit* allows for the identification of a reliable measurement range in a microfluidic channel with a temperature gradient, while accounting for fluid dynamics, heat transfer, and mass transfer characteristics. The proposed approach is validated through rigorous simulations and experiments, enabling an evaluation of the impact of *figure of merit*-derived parameters on the measurement channel. The findings from our study demonstrate that the *figure of merit* serves as a representative measure for stable thermophoretic measurements in a microfluidic channel. Moreover, we propose a threshold value that signifies the transition from a diffusion-dominant to a convection-dominant field.

1. Introduction

Thermophoresis, or thermodiffusion, attracts attention in various fields including geology, biotechnology, engineering, and fundamental science [1, 2]. This phenomenon refers to mass transport in a non-isothermal temperature field, which is different from thermal diffusion, indicating the temperature propagation with time [3]. Often, the terms thermodiffusion and thermophoresis are used interchangeably [4]. However, thermodiffusion refers to the formation of a concentration gradient as a result of a thermal gradient in solutions, while thermophoresis describes the migration of colloidal particles in a fluid due to the presence of a temperature gradient. The Soret coefficient, a measure of thermodiffusion also known as thermophoresis for larger colloidal particles, is influenced by different properties of the fluid and the particle surfaces. For this reason, thermodiffusion is used in various areas. It is discussed in petrology, in petroleum reservoirs, where it influences the distribution of crude oil components [5]. Additionally the accumulation of organic molecules in hydrothermal vents is discussed, which is relevant to the origin of life [6, 7]. The most important application is using the Soret coefficient's potential in studying the binding affinity between ligands and proteins, which holds promise for advancements in drug discovery [8, 9, 10, 11, 12, 13, 14]. Further, studies have shown that thermophoresis can enhance the power factor in thermoelectric materials, enabling the conversion of waste heat into electricity [15, 16, 17]. Despite these promising applications, our understanding of thermophoretic behavior in fluids remains limited, and further development of the underlying theoretical concepts is necessary. The understanding of thermophoretic processes in binary mixtures is currently at a rudimentary stage. However, when dealing with real systems like protein solutions and colloidal suspensions, the complexity increases further due to their multicomponent nature, which can give rise to cross effects [5]. To address these challenges and enable the study of phenomena such as thermodiffusion of colloidal particles in non-isothermal conditions, there is a growing demand for simpler and more quantitative measurement techniques compared to traditional approaches [5, 18, 19, 20, 21]. Microfluidic devices have emerged as prominent tools for investigating transport properties of colloidal particles, encompassing electrophoresis, dielectrophoresis, diffusiophoresis, and especially thermophoresis [22, 23, 24].

Thermophoresis can be described by the following equation [25]:

$$\vec{j} = -\rho D \nabla c - \rho c(1-c) D_{\mathrm{T}} \nabla T \tag{1}$$

In this equation, $\vec{j}$ represents the net mass flux, ρ is the mass density of the particles, D is the diffusion coefficient, c is the solute concentration, D_{T} is the thermodiffusion coefficient, and T is the temperature. The Soret coefficient, S_{T}, can be defined as $S_{\mathrm{T}} = D_{\mathrm{T}}/D$ in steady-state conditions, which is evaluated from the ratio between the induced concentration gradient and the applied temperature gradient. To

*Corresponding author
nk.lee@yonsei.ac.kr (N. Lee); s.wiegand@fz-juelich.de (S. Wiegand)
ORCID(s):

measure the Soret coefficient of particles, various measurement techniques have been introduced such as thermal lens (TL) [26, 27], Thermal Diffusion Forced Rayleigh Scattering (TDFRS) [28, 29], beam deflection [30, 31, 32], and thermogravitational columns (TCs) [33] relying on optical detection, utilizing the refractive contrast caused by temperature and concentration gradients in the system. However, these techniques are limited to binary or specific ternary mixtures, making it challenging to analyze the thermophoretic behavior in multi-component systems. Although TCs can be used to study multi-component systems, they require large sample volumes (around 30 mL) and considerable time to reach equilibrium [33].

To overcome these limitations in measuring the Soret coefficient, the use of micron-sized devices has been proposed [34, 9, 35, 36]. These devices offer advantages such as reduced sample volume requirements and shorter equilibrium times compared to conventional measurement systems. They are particularly useful for thermophoresis in non-isothermal areas and enable efficient particle separation due to the sensitivity of thermophoresis to various parameters [37, 38, 39]. In addition, they also facilitate specific signal detection from colloidal particles, allowing thermophoretic measurements in multi-component systems through direct observation or the use of fluorescent dyes. Researchers have actively advanced microfluidic devices with dedicated channels for temperature gradients [34, 35, 36, 40, 23, 41] to assess the thermophoresis of particles. These cells possess a straightforward configuration that enables direct particle observation or fluorescence signal measurement within the channel. However, it is essential to acknowledge that the temperature gradient direction in these microfluidic cells is perpendicular to the force of gravity, leading to natural convection phenomena occurring within the microfluidic channel.

To obtain reliable Soret coefficient, it is essential to make the concentration and temperature fields only caused by the thermophoresis and the heat conduction using Eq.1. However, a larger temperature gradient can induce a greater concentration gradient, but it also leads to stronger natural convection within the channel, resulting in vigorous mixing [42]. Moreover, manufacturing micron-sized structures can be challenging, often resulting in size deviations within the measurement channel. Consequently, larger microfluidic channels are sometimes used to accommodate these deviations. However, larger channels also amplify natural convection, hindering the study of thermophoretic behaviors within the channel. Therefore, in order to address these conflicting factors in the microchannel with the temperature gradient, it is necessary to establish design criteria that consider various parameters. This involves performing a "thermal design" to extract critical values required for stable measurements [43].

In this study, we present a thermal design guideline for a non-isothermal microfluidic channel to ensure accurate thermophoretic measurements of colloidal particles. We employ dimensional analysis of the governing equation to establish a design parameter, denoted as α, which combines information on channel geometry, properties such as diffusion coefficient and Soret coefficient, and the applied temperature gradient. To validate the model's accuracy, we compare results from multi-physics simulations with experimental data. Additionally, we investigate the influence of these parameters on the thermophoretic field within the measurement channel. Ultimately, our findings demonstrate that the *figure of merit* α can effectively determine stable operation and serve as a *figure of merit* for judging the reliable measurement of the thermophoresis.

2. Method and Materials

2.1. Geometry

Figure 1 illustrates the schematic of microfluidic devices with the temperature gradient (thermophoretic microfluidic cells) in a previous publication [23]. These cells consist of three channels: a heating channel, a cooling channel, and a measurement channel. The heating and cooling channels generate a temperature gradient within the measurement channel. The flow within the channels is counter-flow, ensuring a constant temperature gradient along the measurement channel [3]. The temperature gradient can lead to a complicated distribution of temperature and concentration due to the coupled heat and mass transfer by thermophoresis and natural convection. To reduce complexity and achieve accurate quantitative analysis, it is crucial to design microfluidic devices in such a way that a 1D temperature gradient is established. The temperature gradient can happen in three dimensions, such as the channel width, height, and longitudinal length. Previous research demonstrated that the temperature gradient across the channel width is dominant by comparing such gradients along the channel height and the longitudinal length. For this reason, this study only considers the 2D dimension because the 3D thermal-fluidic behaviors can be negligible.

Typically, natural convection is associated with an up-down flow configuration, where the bottom surface is heated while the top surface is cooled [44]. However, in our case, the transverse direction of the temperature gradient, which is perpendicular to the force of gravity, makes natural convection more prominent compared to the vertical direction. The buoyancy of the fluid in the measurement channel on the cold and hot side causes natural convection, which flattens the concentration gradient and influences the measured Soret coefficient. Therefore, when measuring the Soret coefficient, it is crucial to consider the impact of natural convection.

We set the reference channel dimensions to 100 μm in width and 100 μm in height, and varied the dimensions of each side from 50 μm to 400 μm. The temperature gradient magnitude along the longitudinal direction is small enough to be ignored. Thus, the geometry of this study is 2D, with square and rectangular shapes.

2.2. Simulation

To comprehensively assess the thermophoretic behavior, it is crucial to consider fluid dynamics, heat transfer, and

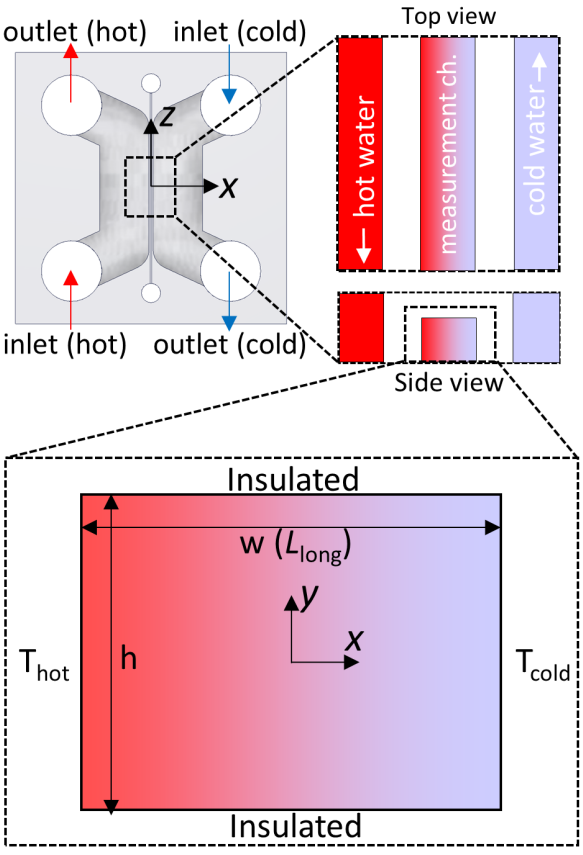

Figure 1: Schematic of the non-isothermal microfluidic channel's geometry for simulation purposes. In this figure, the longest side of channel L_{long} is the width w.

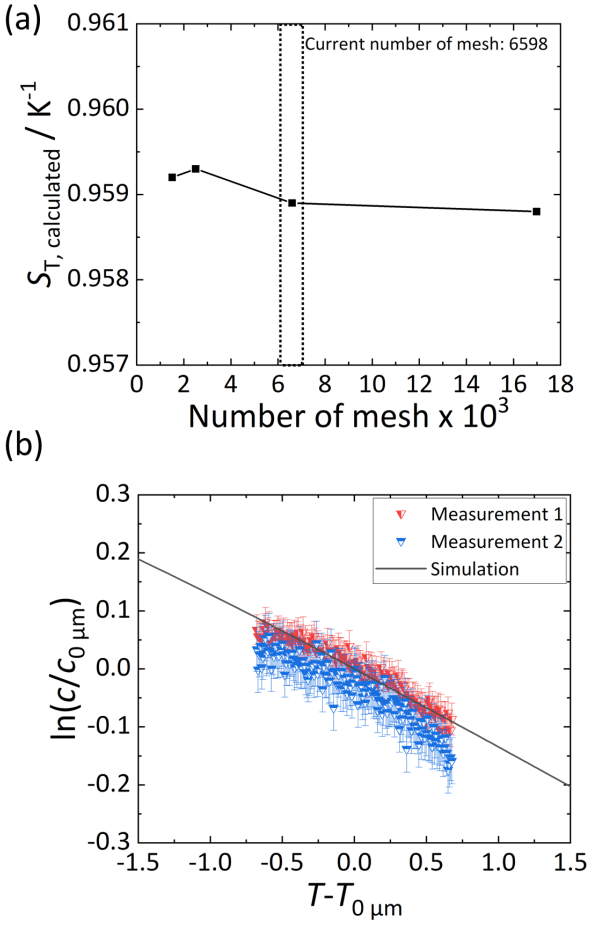

Figure 2: (a) Grid independence test for the simulation. (b) Validation of the simulation through comparison with measurement results.

mass transfer simultaneously. To consider all these factors, we utilize COMSOL Multiphysics v 5.6a, a commercial code, to simulate the thermophoretic behavior under steady state conditions. Using the non-isothermal flow module, we can effectively solve for the fluid and thermal behaviors within the microfluidic channel. The governing equations for the fluid and thermal phenomena are described as follow:

$$\rho \nabla v = 0 \tag{2}$$

$$\rho(v \cdot \nabla)v = \nabla[-pI + K] + F + (\rho - \rho_{ref})g \tag{3}$$

$$\rho C_p v \cdot \nabla T = k\nabla^2 T \tag{4}$$

with the fluid density ρ, the fluid velocity v, the pressure p, the viscous term K, the external force on the fluid element K, the gravity g, the specific heat C_p and the temperature T. The boundary condition for the fluid on all four sides is a no-slip wall condition. One point is designated with the reference pressure of 1 atm. Due to the incompressible flow, the gravitational force is modeled with the Boussinesq approximation. It allows us to describe the change in density of water based solely on the temperature difference [3].

As thermal boundary conditions, the left side represents the hot wall and the right side the cold wall. The upper and lower walls are assumed to be adiabatic, as we have already demonstrated the independence of the temperature distribution in the previous publication [23]. The temperature in the middle is fixed at 20°C. To obtain a consistent thermophoretic behavior, the temperature gradient is fixed at 0.05 K/μm by regulating the temperature of the left and right sides under the reference condition. This means that as the width of the channel increases, the temperature difference within the channel must also increase to compensate for the change in width.

Since we are dealing with a dilute solution (c≪1), we assume that the working fluid is water. For the liquid and thermal behavior, properties such as density, dynamic viscosity, thermal conductivity and heat capacity at constant pressure are required. These properties were integrated into the solver, taking into account temperature-dependent variations, since natural convection is induced by the density differences under non-isothermal conditions. To establish a link between the fluid and thermal results and the mass transfer, we used the PDE module and integrated the following

conjugate equations:

$$-D\nabla^2 c - DS_{\mathrm{T}} c(1-c)\nabla^2 T + v\nabla c = 0 \tag{5}$$

with the diffusion coefficient D, the concentration c, the Soret coefficient S_{T}, the temperature T and the velocity v, respectively.

To assess the influence of the grid points on the calculated Soret coefficient, we first varied the total number of meshes in the simulation. Specifically, we set the number of meshes within the COMSOL module between 1000 and 16000 meshes. The Soret coefficient to evaluate the mesh independence test was determined by analyzing the slope between the log concentration ratio and the temperature difference. Figure Figure 2(a) shows that a convergent result is obtained when the mesh number exceeds 6598. Therefore, we set the current mesh number to 6598. The relatively small number of meshes is due to the 2D simulation, which requires fewer meshes to accurately simulate fluid dynamics, thermal behavior, and mass transfer simultaneously. These convergence limits were set to 0.001, as the combined behavior is very sensitive to further reductions in size.

Additionally, we compare our simulation results with the experimental data for the validation [23]. The compared results are the logarithmic concentration ratio with the temperature difference at the center position. Figure 2(b) demonstrates that simulated results closely overlap with experimental findings from previous research [23]. Based on these findings, we can confidently conclude that the simulation can estimate securely the thermophoresis occurring within the measurement channel.

2.3. Data evaluation

In the steady state of a diluted solution ($c \ll 1$), the flux equation in Eq. 5 can be expressed as:

$$\nabla c = -cS_{\mathrm{T}}\nabla T, \tag{6}$$

with the temperature T and the Soret coefficient S_{T}. In the measuring channel, a one-dimensional temperature gradient occurs along the transverse direction of the channel. Therefore, we can focus solely on the center line of temperature and concentration when evaluating the Soret coefficient. We rearranged Eq.6 into 1D equation using $\nabla c = dc/dx$ and $\nabla T = dT/dx$ as follows:

$$\ln \frac{c(x)}{c(x_{\mathrm{x=0}})} = S_{\mathrm{T}}(T(x_{\mathrm{x=0}}) - T(x)) \tag{7}$$

Based on equation 7, the logarithmic concentration ratio exhibits a linear dependence on the temperature difference $T(x_{\mathrm{ref}})$ - $T(x)$. This implies that the slope of the linear relationship corresponds to the Soret coefficient. Thus, the calculated Soret coefficient was compared to the input value which was used to simulate the thermophoretic behavior under different conditions.

2.4. Dimensional analysis

The thermal, fluid, and mass transfer phenomena in thermophoresis are interconnected, resulting in the generation of concentration gradients due to temperature gradients. Therefore, when designing microfluidic devices with temperature gradients, it is essential to account for natural convection occurring within the measurement channel. This consideration ensures a comprehensive understanding of the conjugated behavior and facilitates the optimization of device performance. To analyze the natural convection effect in the micron-sized chamber or channel, several researchers tried to utilize the threshold value based on a Rayleigh number of 2300 [44]. This crucial value arises from the assumption that the hot plate is positioned at the bottom while the cold plate is located at the top. It means that the temperature gradient direction is counter-direction with the gravity field. For this reason, if the micron-sized chamber satisfies this threshold with the same temperature configuration, it guarantees the stability of the flow field against natural convection within the chamber. Otherwise, many researchers make different temperature configurations that are hot on the top side and cold on the bottom side [36].

However, in the non-isothermal microfluidic channel for measuring thermophoretic properties, the temperature field aligns vertically with the gravity direction due to the horizontal orientation of the temperature and concentration measurements [45, 46]. This configuration facilitates the natural convection within the non-isothermal microfluidic channel, necessitating consideration of its impact on the measurement. A detailed explanation of the natural convection mechanism can be found in reference [3]. We will specifically focus on the hot wall and its role in the natural convection mechanism to gain a deeper understanding. For this analysis, we can leverage the momentum equation to identify the driving source of natural convection. From the reference [3], the momentum equation on the differential control volume along the horizontal direction (x) in the presence of a horizontal temperature gradient can be written as follows:

$$u\frac{\partial u}{\partial x} + v\frac{\partial u}{\partial y} = \nu\frac{\partial^2 u}{\partial y^2} + g\beta(T - T_{\mathrm{inf}}). \tag{8}$$

where u, v, ν, x, y, g, β, T and T_{inf} are the horizontal velocity, the vertical velocity, the kinematic viscosity, horizontal axis, vertical axis, gravity, the volume expansion coefficient, the fluid temperature of differential control volume and the ambient fluid temperature.

The second term on the right-hand side of the governing equation represents the net force along the horizontal direction (x-axis) resulting from the change in volume (density) due to the temperature gradient. This force acts as an initial ignition for natural convection. It causes a buoyant flow along the vertical direction (y-axis) as the fluid element affected by the hot wall moves away due to the horizontal momentum gained and its lower density compared to the surrounding fluid. As a result, the cumulative increase in volume of these affected fluid elements expands the boundary layer from the lower edge to the upper edge of the hot wall. It implies that the natural convection along the vertical direction happens through the accumulation of

volume (density)-changed fluid elements from the bottom to the top. At the cold wall, a reverse process takes place, which means that the volume (density)-changed fluid started from the cold wall's top wall to the cold wall's bottom wall. This highlights the importance of considering natural convection simultaneously with the temperature and concentration measurements in the channel, even when the gravity and temperature gradient are perpendicular. Additionally, the aforementioned threshold value [44] is not applicable in microfluidic channels with temperature gradients. Thus, other factors must be considered to determine the relative significance of diffusion with thermophoresis compared to natural convection.

To begin with, based on the governing equation stated in Equation 5, we initially assume that mass transfer resulting from thermophoresis predominantly occurs along the x-direction, leading to the concentration gradient primarily existing along the x-axis. Additionally, due to buoyancy effects, we guess that the fluid velocity along the y-axis can be greater than the fluid velocity along the x-axis, as gravity acts in the direction of the y-axis. Furthermore, it is important to note that the solution's concentration is sufficiently dilute ($c \ll 1$). Consequently, Equation 5 can be expressed in the following manner:

$$-D\frac{d^2c}{dx^2} - DS_{\mathrm{T}}c\frac{d^2T}{dx^2} + v\frac{dc}{dx} = 0. \tag{9}$$

The first term in the equation represents the diffusion process, the second term accounts for the thermophoretic behavior, and the third term corresponds to the convection process. Then, we perform the dimensional analysis by changing appropriate variables in the governing equation into the geometrical and operating parameters. x is the longest side of channel L_{long} in the cross-sectional plane, which is the width w in Fig. 1. T is the temperature difference ΔT in the channel. c is the initial concentration c_0. v is the maximum velocity $|v_{nc,max}|$ induced by natural convection. S_{T} is the absolute value of the Soret coefficient $|S_T|$ of the solute. By substituting the values in the Eq.9, we arrange the Eq. 10 as follow:

$$\alpha \sim \frac{v_{nc,max}}{\frac{D}{L_{\mathrm{long}}}(1 + |S_{\mathrm{T}}|\,\Delta T)} \tag{10}$$

Here, $v_{nc,max}$ represents the maximum velocity induced by natural convection, D is the diffusion coefficient, L_{long} is the longest channel length in the cross-sectional plane, $|S_{\mathrm{T}}|$ is the absolute value of the Soret coefficient, and ΔT is the temperature difference in the channel. Note that the natural convection velocity occurs in the whole channel, and the temperature-dependent properties determine fluidic behaviors in the channel. However, only the temperature and concentration fields at the center part of the channel are used for evaluating the thermophoretic properties. Therefore, we use the diffusion coefficient at the center of the channel corresponding to the average temperature for the figure of merit.

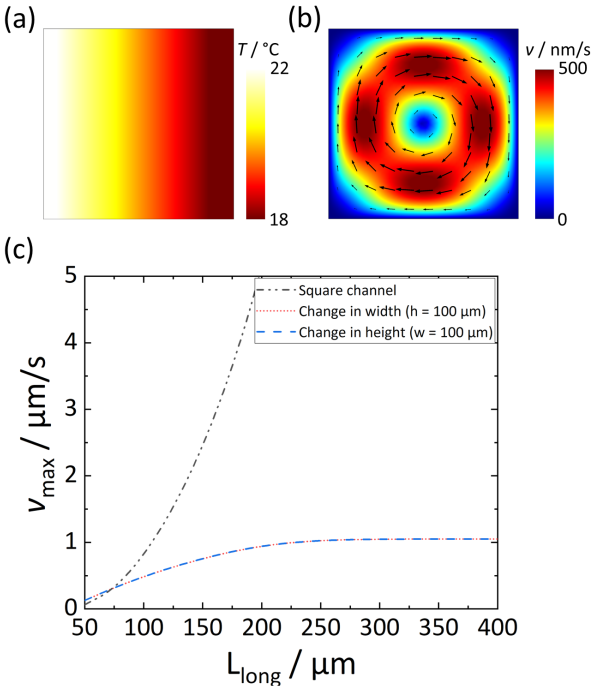

Figure 3: (a) Distribution of temperature and (b) distribution of velocity within the cell. (c) Variation of the maximum velocity caused by natural convection as the width, height, and side length of the square channel change.

We introduce a factor α as a "figure of merit" to effectively design a microfluidic channel with a temperature gradient that can reliably measure thermophoretic properties. The value of α holds significant implications for the thermophoretic behavior within the system. When α is considerably smaller than 1, thermophoresis becomes dominant, enabling the measurement of Soret coefficients through the channel. On the contrary, when α is significantly larger than 1, convection prevails, leading to constant concentration due to intense mixing. As a result, the channel becomes unsuitable for accurate measurements. When α is around 1, careful consideration is required to determine the functionality of the microfluidic channel as a measurement device. For this reason, we assert that α serves as a reliable design criterion for the non-isothermal microfluidic channel for measuring thermophoretic properties.

3. Results and Discussion

3.1. Natural convection characteristics depending on geometrical and operating factors

The factor α contains various pieces of information such as the maximum natural convection velocity, the diffusion coefficient, the channel width, Soret coefficient and the temperature differences. The natural convection velocity, unlike the other factors, needs to be separately calculated through simulation. This is because estimating the velocity is

challenging due to the complex nature of natural convection within confined geometries. Therefore, in order to account for this, we assessed the maximum natural convection velocity based on simulated results. This approach was chosen as it validates the combined impact of natural convection and thermophoresis using experimental data from the previous section.

The dominant factor influencing natural convection in the microchannel is its geometrical configuration, as the flow acceleration due to the buoyancy being constrained by dimensions of each side. Figure 3(a) illustrates the temperature distribution within the measurement channel. Previous studies have demonstrated that the temperature remains independent along vertical and longitudinal directions [23]. This characteristic allows for the simulation of thermophoretic behavior in the measurement channel using 1D temperature distribution. Consequently, we computed the natural convection shown in Fig. 3(b) based on this 1D temperature distribution. In Fig. 3(b), we observe that the density of water decreases at the hot wall (left side), resulting in an upward flow. Simultaneously, the density of water increases at the cold wall (right side), leading to a downward flow. These flows accelerate and decelerate before reaching the wall, as the fluid velocity must be zero at the stagnation point. Subsequently, the flows make a 90° turn and undergo re-acceleration and deceleration in the transverse direction within the channel. This continuous process generates flows from each side wall through natural convection. At the center of the channel, there is a balancing effect between the upward flow at the hot wall and the downward flow at the cold wall, resulting in the cancellation and neutralization of fluid velocity. Analysis of the contour reveals that the maximum velocity occurs at the midpoint of each side.

Utilizing simulation results, we present the maximum velocity of natural convection for inserting α in Fig. 3(c). To alter the maximum natural convection velocity within the channel, we adjust geometric dimensions of the cell due to their significant correlation with natural convection. We consider different cases for simulation, including a square-shaped and a rectangular-shaped measurement channel. The square channel serves as the reference channel, with each side having the same length. On the other hand, the rectangular channel is employed to investigate the effect of confinement, which restricts the flow acceleration due to natural convection. In all cases, the dimensions of the reference channel are 100 μm (width) by 100 μm (height). Using this reference channel size as a baseline, we vary the width from 50 μm to 400 μm and the height from 50 μm to 400 μm.

To enable a comparison between different sizes, we utilize the length of the longest side as the parameter on the x-axis. As shown in Fig. 3(c), it becomes evident that the maximum natural convection velocity exhibits a direct proportionality to the longest side within the measurement channel. Notably, the slope of the square channel, representing the longest side, is steeper than that of the rectangular channel. When varying each side length of the square channel from 50 μm to 400 μm, the maximum velocity experiences a range of variation from 0.064 μm/s to 32.9 μm/s. On the other hand, in the case of a rectangular channel, regardless of its vertical or horizontal orientation, the maximum natural convection velocity ranges from 0.127 μm/s to 1.05 μm/s. This observation highlights the strong confinement effect presented in the rectangular channel, which diminishes the natural convection velocity within the measurement channel. Consequently, the acceleration of the natural convection velocity along the hot and cold walls is hindered. This indicates that the natural convection can be controlled by adjusting the confined length of the channel, allowing for an increase in the size of the measurement section. Since the natural convection impedes the desired thermophoretic behavior in the channel, such confinement on the natural convection is beneficial.

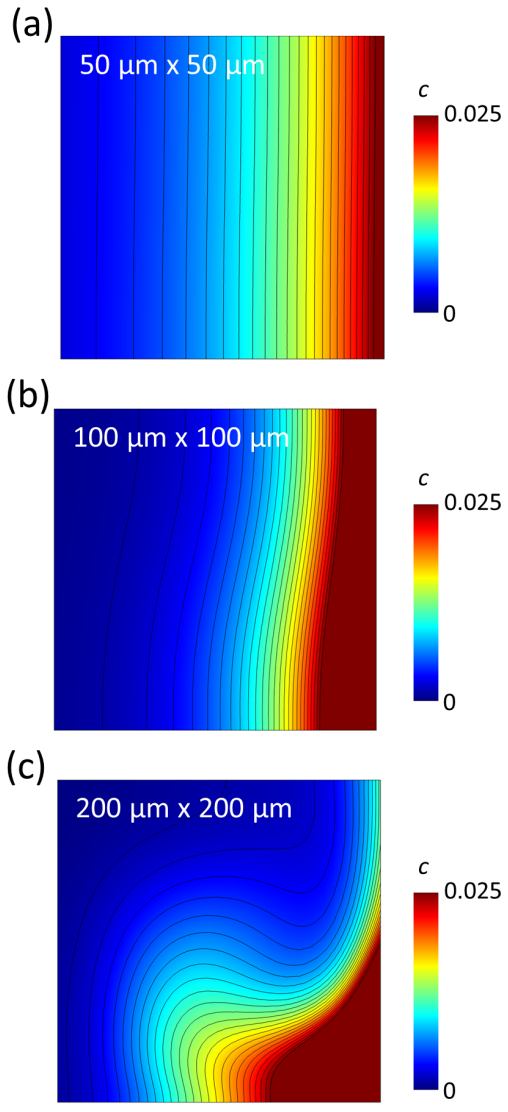

Figure 4: Concentration distribution with varying sizes of square channels: (a) 50 μm x 50 μm, (b) 100 μm x 100 μm and (c) 200 μm x 200 μm.

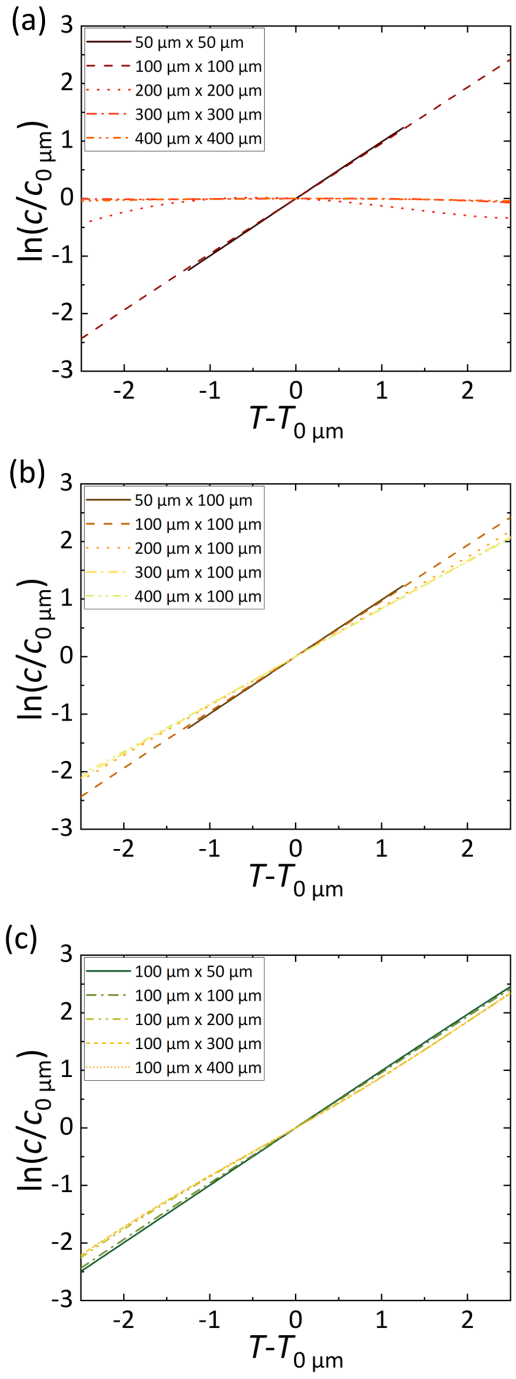

Figure 5: Logarithmic concentration ratio as a function of temperature difference for different variations in (a) square size, (b) width, and (c) height.

Based on the natural convection behavior, we perform a conjugate analysis including the mass transfer. We assume that D represents the Einstein diffusion coefficient of colloidal particle with a diameter of 10 nm in water. Additionally, the Soret coefficient is assumed to be 1 K^{-1}, and there is a temperature gradient of 0.5 K/μm. Figure 4 shows the concentration distribution in the measuring channel with the natural convection. Figures 4 (a), (b) and (c) correspond to the actual size of the contour despite the increase in the side length of the square channel. We understand that the concentration distribution is mixed with the enlargement of the channel. This explains that the advection term dominates the field in Eq.5, which results in the unreliable-thermophoretic measurement channel. To compare the mixing effect on measuring Soret coefficient quantitatively, we arrange the logarithmic concentration distribution with the temperature difference based on Eq.7. Figure 5(a) shows the logarithmic concentration ratio as a function of the temperature difference for different channel sizes. In the graph, the slope between the logarithmic concentration ratio and temperature difference expresses the Soret coeffcient. Based on our findings, we can conclude that channel sizes exceeding 200 μm by 200 μm cannot yield reliable Soret coefficients in the measurement channel. This limitation arises from the homogenization caused by convection, resulting in a zero-slope condition. Figure 5 (b) and (c), however, show the linear relation between the logarithmic concentration ratio and the temperature difference despite to the increase in the longest side of the rectangular channel. Even though the discrepancy increases with the increment in the longest length, the diffusion determines the concentration field in the measurement channel which can provide reliable measurements of the Soret coefficient. It means that if we confine one side of the rectangular channel, then the measurement channel works properly. In addition, the increase in channel size induces the convection dominated channel which cannot provide the Soret coefficient. To obtain a general description of various parameters, we apply dimensional analysis to convert geometric factors into a dimensionless parameter called α. In Figure 6(a) we see the dependence of α on the longest length of the measurement channel for both square and rectangular channels. As shown in Fig. 6(a), the value of α increases abruptly with increasing length of the longest channel for the square channel. However, for the rectangular channel, α increases steadily with increasing channel width and height, while it remains proportional to the longest channel length. This behavior indicates that α adequately captures the variation in natural convection velocity. Figure 6(b) presents a comparison between the Soret coefficient calculated from simulated results and the input Soret coefficient used in the thermophoresis simulation. The unity value corresponds to an identical match between the input value and the calculated Soret coefficient. As illustrated in Fig. 6(b), when α increases, a significant deviation occurs in the graph beyond a certain threshold value around unity. In dimensional analysis, we propose that when the threshold value, which is approximately *one*, is reached, it causes a shift from diffusion-dominated terms to convection-dominated terms in Equation 5. Although the threshold value may not precisely be unity, as α approaches zero, the deviation of the Soret coefficient also approaches zero. α values above *one* exhibit substantial deviations in the Soret coefficient, resulting from convection leading to mixing within the measurement channel. Hence, we can conclude that the parameter α effectively represents the

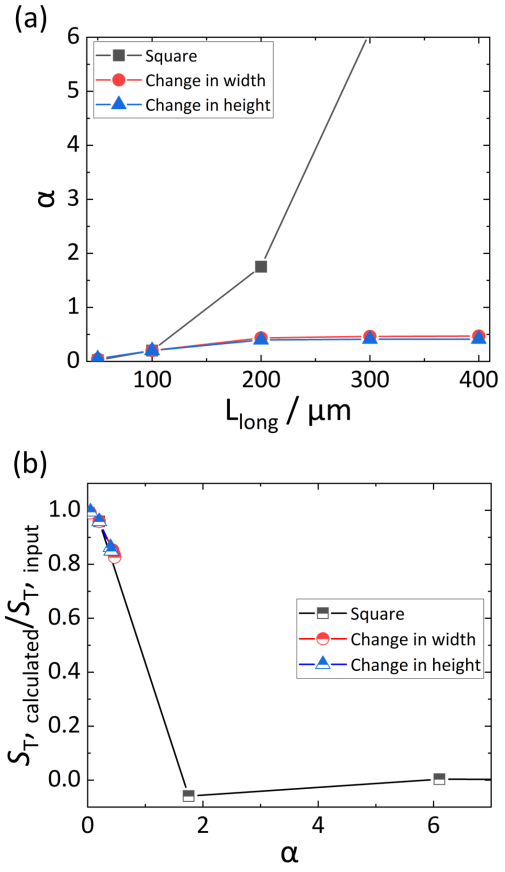

Figure 6: Graphs depicting the relationship between (a) the longest size of the channel and alpha (α), and (b) the relationship between alpha (α) and the calculated Soret coefficient (S_T) derived from the simulation.

range whether thermophoretic measurements yield reliable Soret coefficient or not. To analyze the influence of other parameters on α, we investigate variations in operating conditions such as temperature difference, as well as properties including diffusion coefficient and Soret coefficient.

3.2. Operating and property effect on the thermophoretic behavior

Initially, we focus on investigating the influence of the temperature gradient on the thermophoretic behavior within the measurement channel. The temperature gradient is a controlled factor achieved by adjusting the temperatures of hot and cold water. The channel size is set to 100 μm by 100 μm, while the diffusion coefficient corresponds to the Einstein diffusion coefficient for colloidal particles with a diameter of 10 nm in 20°C water. The Soret coefficient is fixed at 1 K^{-1}, and the average temperature is 20°C. In a previous study [42, 23], reducing the wall thickness below 100 μm proved to be challenging. This led to a significant temperature drop at the wall, resulting in a maximum temperature gradient of approximately 0.1 K/μm in the measurement channel. Thus, we consider a temperature gradient range from 0.025 K/μm to 0.1 K/μm, with a reference value of 0.05 K/μm. Figure

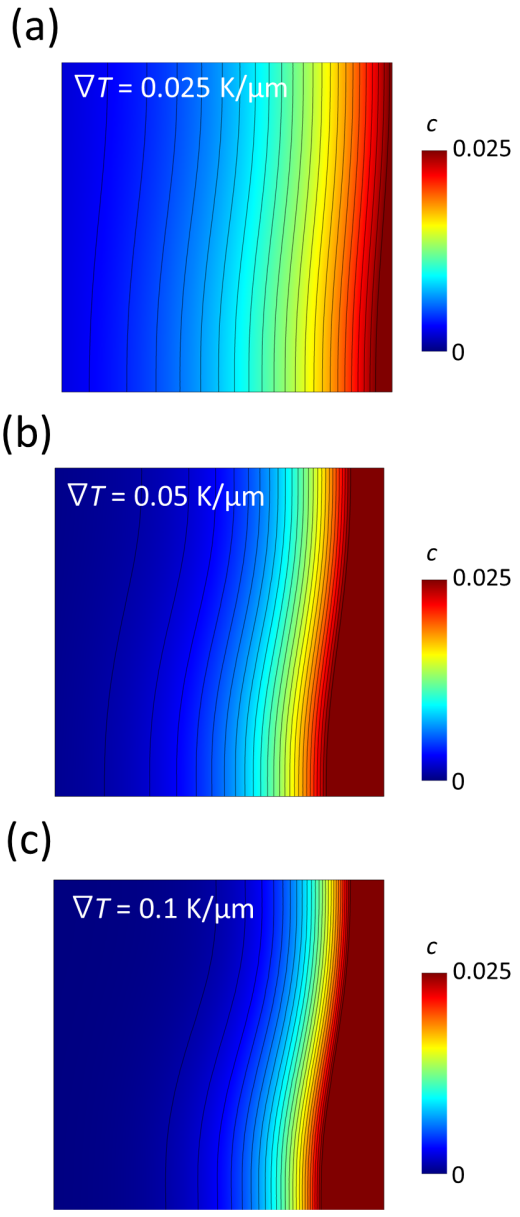

Figure 7: Effect of temperature gradient on concentration distribution in case of (a) ∇T = 0.025 K/μm, (b) ∇T = 0.05 K/μm and (c) ∇T = 0.075 K/μm

7 illustrates the concentration distribution depending on the temperature gradient. As shown in Fig. 7, an increase in the temperature gradient leads to a corresponding increase in the concentration gradient. According to the relationship $S_T \cdot dT \sim dc/c$, a larger temperature gradient induces a larger concentration gradient within the measurement channel, assuming a constant Soret coefficient. To assess the temperature gradient's effect on the thermophoretic field, we calculate the Soret coefficient from the slope between the logarithmic concentration ratio and the temperature difference within the channel. Figure 8(a) presents a quantitative comparison of the logarithmic concentration ratio with the temperature difference for different temperature gradients.

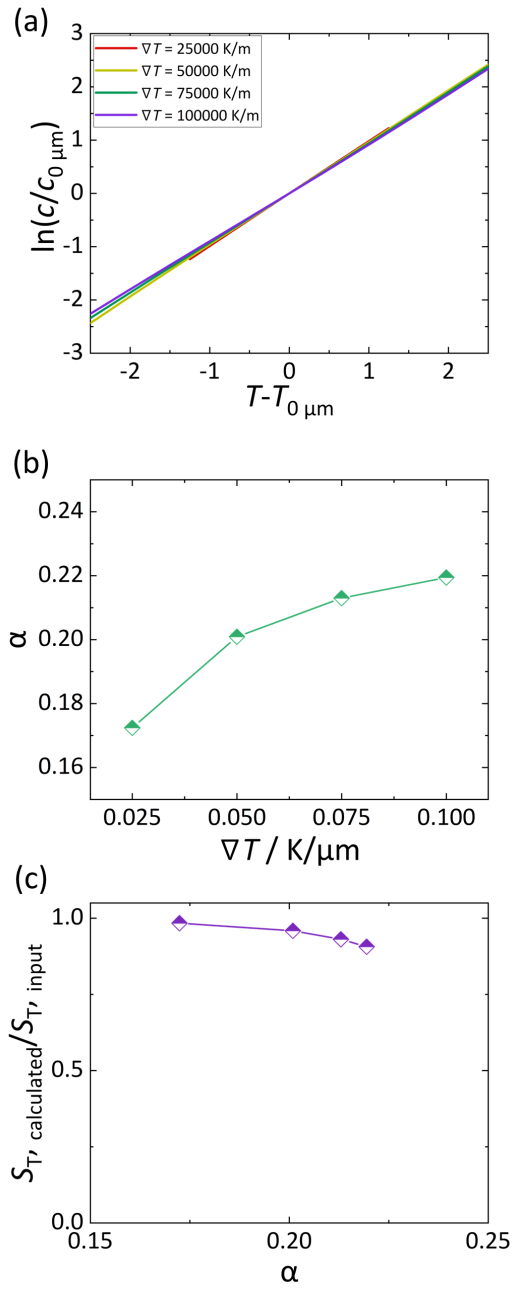

Figure 8: (a) Logarithmic concentration ratio as a function of temperature difference for various temperature gradients within the cell. Graphs depicting the relationship between: (b) Temperature gradient and α, and (c) α and the calculated Soret coefficient.

The graphs have similar slopes, which makes it challenging to distinguish any significant differences between them. This suggests that the effect of the temperature gradient is relatively weak since it increases both the natural convection velocity and the thermophoretic effect in the field simultaneously. To summarize these findings in terms of α, we present Figs. 8(b) and (c) to evaluate the parameter's effect on α and the deviation of the Soret coefficient. Depending on the temperature gradient, α ranges from 0.17 to 0.22,

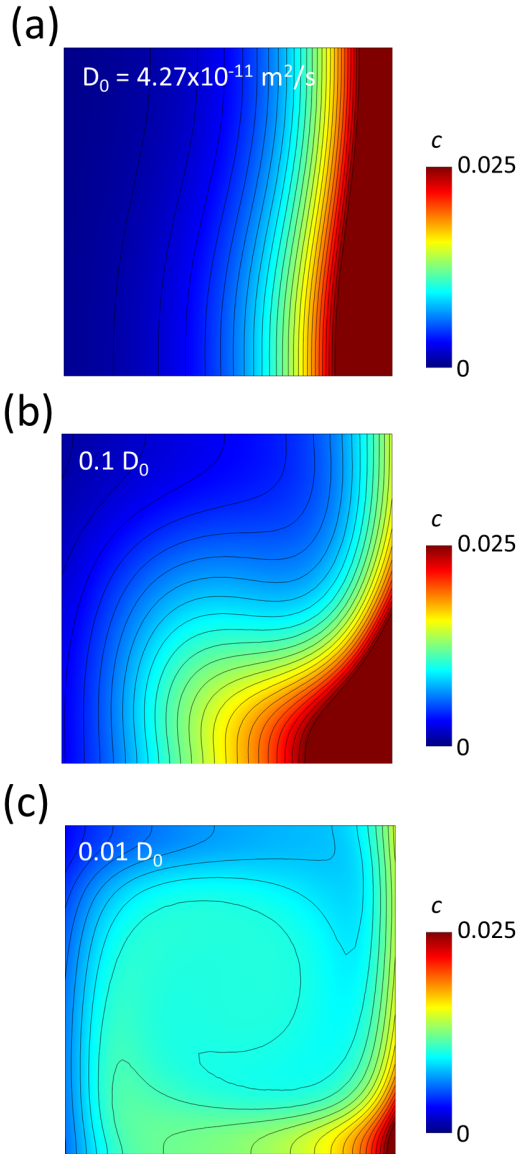

Figure 9: Influence of the diffusion coefficient on the concentration distribution for three scenarios: (a) $D_0 = 4.27 \times 10^{-11}$ m^2/s, (b) $0.1 \cdot D_0$, and (c) $0.01 \cdot D_0$

which is significantly lower than 1. This indicates that the dominant behavior in the channel is diffusion, as depicted in Fig. 8(c), where the discrepancy of the Soret coefficient remains within 10% of the input value.

Another influential factor contributing to α is the diffusion coefficient, which is directly linked to the concentration gradient field in the presence of a temperature gradient. Hence, it is important to examine the impact of the diffusion coefficient on the thermophoretic field within the channel. As before we use the diffusion coefficient of a 10 nm bead in water at 20°C as reference. By increasing the colloid diameter, we vary the diameter from 10 nm to 1000 nm, resulting in a corresponding change in the diffusion coefficient from D_0 (d = 10 nm) to 0.01 D_0 (d = 1000 nm). Figure 9 illustrates the concentration field as function of the diffusion coefficient.

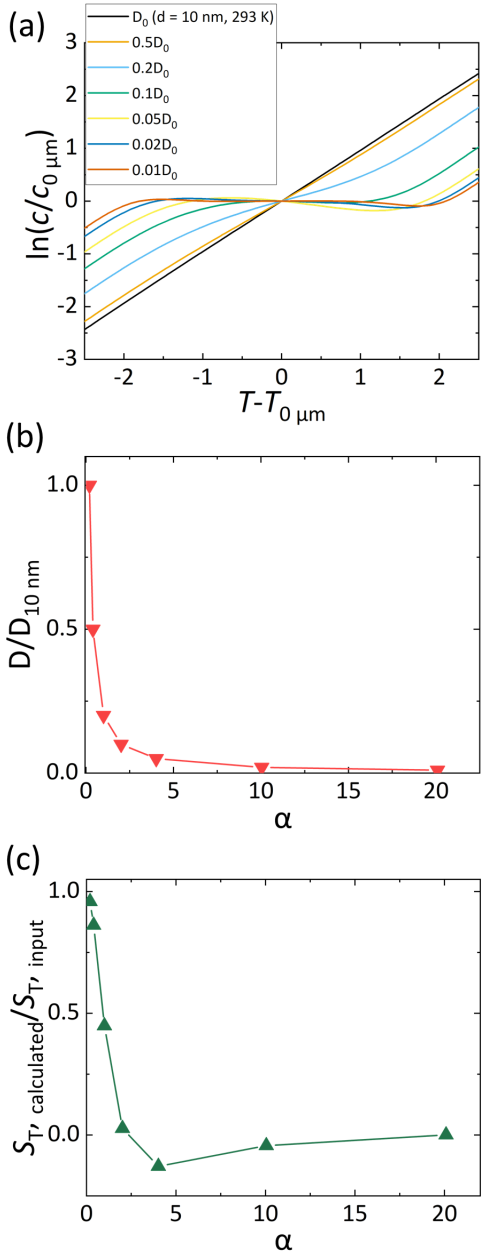

Figure 10: (a) Logarithmic concentration ratio as a function of temperature difference, considering variations in the diffusion coefficient relative to the Einstein-diffusion coefficient of a colloidal particle with a diameter of 10 nm. Graphs depicting the relationship between: (b) α and the ratio of the diffusion coefficient to the diffusion coefficient of a 10 nm bead, and (c) α and the calculated Soret coefficient.

With a larger diffusion coefficient corresponding to a 10 nm diameter, the concentration field is primarily governed by thermophoresis, even in the presence of natural convection within the channel. However, as the diffusion coefficient decreases, an abrupt change occurs in the concentration field within the channel. Particularly, for a colloid diameter of 1000 nm (0.01 D_0), the concentration field becomes nearly flat due to the dominance of strong convection. This indicates that the diffusion coefficient is another crucial factor in determining the criteria for measuring thermophoresis in the channel.

To quantify the relationship between the diffusion coefficient and the Soret coefficient, we plot the logarithmic concentration ratio against the temperature difference for various diffusion coefficients in Figure 10(a). The graph pattern exhibits significant variations depending on the diffusion coefficient. Significantly, when dealing with smaller diffusion coefficients associated with larger particle diameters, the slopes of the graphs decrease and become even slightly negative. Surprisingly, despite inputting a positive Soret coefficient in the simulation, no concentration gradient is observed. This indicates that the prevalence of natural convection can lead to a reversed sign within the channel, making it inappropriate for accurately measuring the thermophoretic field in that particular scenario. Similar to the impact of temperature gradient, we quantify the influence of diffusion coefficient variation by converting it into α, as illustrated in Figure 10(b). It is evident from Fig. 10(b) that α undergoes abrupt change depending on the diffusion coefficient, highlighting the crucial role of the diffusion coefficient in determining the concentration field within the measurement channel. Figure 10(c) displays the ratio of the calculated Soret coefficient to the input value as a function of α. We notice a substantial influence of the diffusion coefficient on the Soret coefficient, indicating that it is another significant parameter that affects the thermophoretic field within the measurement channel. Note that natural convection flattens the concentration profile within the channel and in extreme cases can even reverse the profile due to the rotational flow it causes. This means that a negative value of the concentration ratio (calculated compared to the input) results from the rotational flow caused by natural convection.

The Soret coefficient plays a crucial role as the final determinant of α. Assessing the impact of the Soret coefficient on the thermophoretic field is a complex task due to its dependence on both the diffusion coefficient and the thermodiffusion coefficient. In order to investigate the influence of this parameter, we conduct simulations with varying Soret coefficients and analyze the underlying factors contributing to observed results. The diffusion coefficient corresponds to the Einstein diffusion coefficient for particles with a diameter of 10 nm. The Soret coefficient is set to 1 K^{-1}. The average temperature is 20°C, and the temperature gradient is 0.5 K/μm. Figure 11 illustrates the concentration field within the measurement channel for different Soret coefficients. It can be observed that the magnitude of the concentration gradient in the field is proportional to the Soret coefficient. Consequently, a lower Soret coefficient results in a less pronounced concentration field compared to a higher Soret coefficient, as depicted in Fig. 11. However, even with a small concentration gradient occurring in the channel, it is still possible to estimate the Soret coefficient accurately. Therefore, we proceed to quantify the slope between the logarithmic concentration ratio and the temperature difference

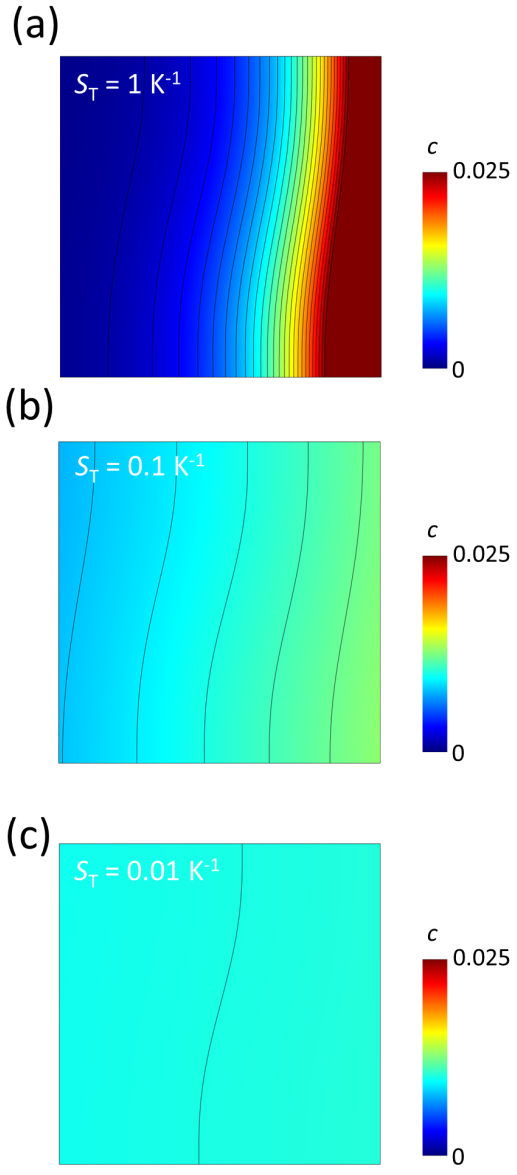

Figure 11: Effect of Soret coefficient on concentration distribution in case of (a) S_T= 1 K^{-1}, (b) S_T= 0.1 K^{-1} and (c) S_T= 0.01 K^{-1}

and compare the quantitative differences depending on the Soret coefficient. Figure 12 presents the ratio of the extracted Soret coefficient to the input value. As evident from the figure, the difference in the Soret coefficient remains small enough to estimate the input value with an error within 10%, even when α exceeds unity. We attribute this effect to the presence of a large diffusion coefficient. In the preceding paragraph, we established that the diffusion coefficient is a dominant factor in determining the thermophoretic field. To compare the Soret coefficients, we employ a diffusion coefficient of D_0, which is sufficiently large to outweigh the small contribution from the thermodiffusion coefficient in the Soret coefficient. This implies that the Soret coefficient is not the primary factor determining the thermophoretic field. Therefore, before measuring colloids to determine the Soret

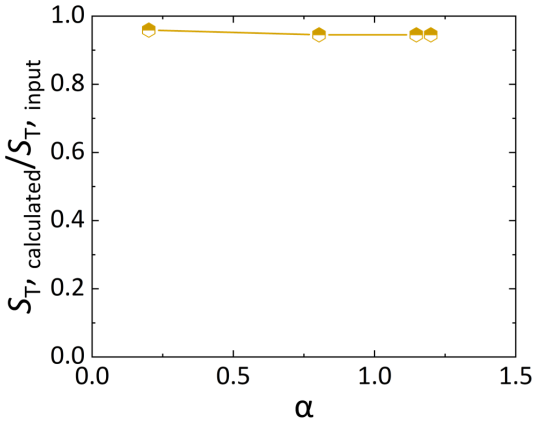

Figure 12: Graph illustrating the relation between α and the calculated Soret coefficient.

coefficient, it is essential to consider the diffusion coefficient of the colloidal particles and ascertain whether they can be accurately measured in the non-isothermal microfluidic channel or not.

Note that the Soret coefficient (S_T), as described in Eq. 1, depends on both the diffusion coefficient (D) and the thermodiffusion coefficient (D_T). A larger Soret coefficient may indicate either an inversely proportional diffusion coefficient or a directly proportional thermodiffusion coefficient. In this work, we analyzed the contributions of the Soret coefficient and the diffusion coefficient separately, since thermophoretic microfluidic cells can only measure the Soret coefficient directly. We plan to conduct a future study in which the diffusion and thermodiffusion coefficients are varied independently.

3.3. Design guideline of non-isothermal microfluidic channel for the thermophoretic measurement

Based on the observed effects of design parameters on the thermophoretic field, it becomes evident that α is a suitable *figure of merit* for capturing the combined influence of natural convection and design parameters. Furthermore, α effectively characterizes the thermophoretic field by representing the ratio between diffusion behavior and natural convection in the field. Consequently, we can gather the parametric studies discussed in the previous section and extract insights for thermal design considerations in the non-isothermal microfluidic channel used for thermophoretic measurements.

Figure 13 gathers calculated results with various parameters and presents the relationship between the calculated and input Soret coefficient ratio and α, which ranges from 0 to 10. α consists of various parameters whic relate to the design of the thermophoretic microfluidic cell. From this figure, we can identify a distinct decrease point occurring around $\alpha = 1$. Below $\alpha = 1$, the calculated Soret coefficient approches to 1. Otherwise, above $\alpha = 1$, the calculated Soret coefficient is close to zero. From the governing equation,

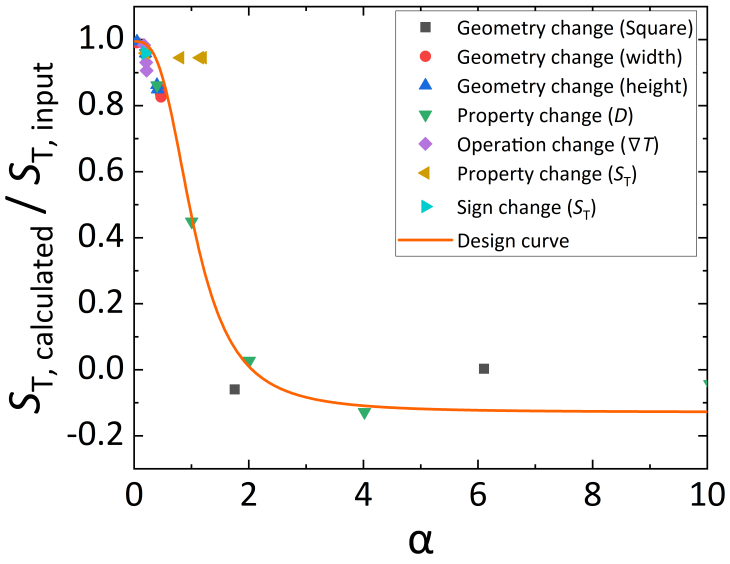

Figure 13: Ratio between the calculated and input Soret coefficient as a function of α (ranging from 0 to 10), influenced by various parameters and designs of the non-isothermal microfluidic channel.

α encompasses the thermal-fluid behavior, including mass transfer, within the measurement channel. For this reason, α can serve as a valuable thermal design guideline as it encompasses a range of information about the parameters, including the maximum natural convection velocity, the diffusion coefficient, Soret coefficinet, geometrical factors, and temperature gradient, simultaneously. To establish a thermal design guideline, we employ a logistic fit to generate a master curve, described by the following equation:

$$y = A2 + (A1 - A2)/(1 + x/x_0)/p \tag{11}$$

where $A1$, $A2$, x_0 and p are the intersection value with y-axis, the lower limit of y-value, the x-value by the half of $A1$ and $A2$, and the power number for fitting the curve. The graph in Figure 13 displays a well-fitted curve that accurately represents the dataset. In this graph, $A1$ is determined to be 0.9945, indicating that as α approaches zero, the calculated Soret coefficient converges to the input Soret coefficient, corresponding to a diffusion-dominant field. The value of x_0 is found to be 1.04, indicating the transition from a diffusion-dominant field to a convection-dominant field at $\alpha = 1.04$. This value holds significant importance as it establishes a clear criterion for non-isothermal microfluidic channel design when aiming to measure the Soret coefficient. Moreover, if α is smaller than unity, the non-isothermal microfluidic channel can successfully measure quantitative data such as the Soret coefficient using various observation techniques. Additionally, this result suggests that non-isothermal microfluidic channel with constrained length in a specific direction can effectively suppress natural convection beyond expectations. This indicates the possibility of increasing the measurement section while reducing the dimensions of other sides to create a diffusion-dominant field. Therefore, α serves as a design guideline for non-isothermal microfluidic channel, enabling the identification of the diffusion-dominant field within the measurement channel.

4. Conclusion

We investigated the design factor to integrate the thermal, fluid and mass transfer behavior in the temperature gradient channel and suggested the design criteria for the non-isothermal microfluidic channel for measuring the Soret coefficient. Using numerical simulations, we accurately modeled and validated multiphysical behaviors occurring in the non-isothermal microfluidic channel. Moreover, by conducting dimensional analysis on the governing equation for thermophoretic behavior in the channel, we can extract the design factor α, which takes into account for operating parameters, properties, and geometrical factors simultaneously. Based on the suggested *figure of merit* α, we simulated the thermophoretic behavior in the channel and observed the threshold to change from the diffusion-dominant field to the convection-dominant field. The results demonstrated a close relationship between the natural convection velocity and the geometrical factors. The natural convection velocity had a significant impact on the thermophoretic field within the measurement channel. Therefore, the geometrical factor, which can be intentionally modified, played a crucial role in determining whether the non-isothermal microfluidic channel could effectively measure the Soret coefficient or not.

In addition, we checked parameters such as the temperature gradient, the diffusion coefficient depending on the diameter of colloidal particle, the Soret coefficient. The results revealed that the diffusion coefficient played a crucial role in determining whether the field was dominated by diffusion

or convection. In conclusion, we propose that α can serve as a useful indicator for designing non-isothermal microfluidic channels, such as thermophoretic microfluidic cells. If α is smaller than or equal to unity, we are in a diffusion-dominant field, which means that it is possible to measure the Soret coefficient in the non-isothermal microfluidic cell. When α exceeded a certain threshold value (unity), a convection-dominant field occurred within the channel. This means that convection hinders the accurate measurement of the thermophoretic effect in the channel. If we cannot judge the figure of merit easily, the longest length on the cross-sectional plane of measurement channel should be below 100 μm [40, 23, 41] which can suppress the natural convection sufficiently as depicted in Fig. 3(c). Note that the figure of merit is difficult to utilize for the non-Newtonian fluid because the fluid velocity varies thermo-fluidic properties, such as viscosity in the non-Newtonian fluid. Consequently, the figure of merit in the current research is limited to Newtonian fluids. If the figure of merit is extended for non-Newtonian fluids, then the thermo-fluidic properties should be well-known for analyzing the figure of merit α, or further studies are needed. This study provides valuable insights into stable measurements studying thermophoretic behavior in microfluidic channels. It enhances our understanding of the thermal, fluid, and mass transfer behaviors occurring in non-isothermal microfluidic channels.

Acknolwedgement

We are grateful to Jan Dhont for inspiring ideas and his generous support of our work. NL acknowledges the support by the Humboldt foundation. This research was supported by the Yonsei University Research Fund of 2023 (2023-22-0160).

CRediT author statement

Namkyu Lee: Conceptualization of this study, Methodology, Measurement, Writing and Editing. **Simone Wiegand**: Data curation, Writing - Original draft preparation

References

[1] M. A. Rahman and M. Z. Saghir. Thermodiffusion or Soret effect: Historical review. *Int. J. Heat Mass Transf.*, 73:693–705, June 2014.

[2] F. M. Coelho, L. F. M. Franco, and A. Firoozabadi. Thermodiffusion of CO2 in Water by Nonequilibrium Molecular Dynamics Simulations. *J. Phys. Chem. B*, 127(12):2749–2760, 2023.

[3] Y. Cengel. *Heat and mass transfer: fundamentals and applications*. McGraw-Hill Higher Education, 2014.

[4] Rodrigo de Miguel and J. Miguel Rubí. Negative thermophoretic force in the strong coupling regime. *Phys. Rev. Lett.*, 123(20):200602, 2019.

[5] W. Köhler and K. I. Morozov. The soret effect in liquid mixtures - a review. *J. Non-Equil. Thermody.*, 41:151–197, 2016.

[6] P. Baaske, F. M. Weinert, S. Duhr, K. H. Lemke, M. J. Russell, and D. Braun. Extreme accumulation of nucleotides in simulated hydrothermal pore systems. *Proc. Natl. Acad. Sci. USA*, 104:9346–9351, 2007.

[7] D. Niether, D. Afanasenkau, J. K. G. Dhont, and S. Wiegand. Accumulation of formamide in hydrothermal pores to form prebiotic nucleobases. *Proc. Natl. Acad. Sci. USA*, 113:4272–4277, 2016.

[8] P. S. Dittrich and A. Manz. Lab-on-a-chip: microfluidics in drug discovery. *Nat. Rev. Drug Discov.*, 5(3):210–218, 2006.

[9] S. A. I. Seidel, P. M. Dijkman, W. A. Lea, G. van den Bogaart, M. Jerabek-Willemsen, A. Lazic, J. S. Joseph, P. Srinivasan, P. Baaske, A. Simeonov, I. Katritch, F. A. Melo, J. E. Ladbury, G. Schreiber, A. Watts, D. Braun, and S. Duhr. Microscale thermophoresis quantifies biomolecular interactions under previously challenging conditions. *Methods*, 59(3):301–315, 2013.

[10] J.-P. Renaud, C.-W. Chung, U. H. Danielson, U. Egner, M. Hennig, R. E. Hubbard, and H. Nar. Biophysics in drug discovery: impact, challenges and opportunities. *Nat. Rev. Drug Discov.*, 15(10):679–698, 2016.

[11] M. Asmari, R. Ratih, H. A. Alhazmi, and S. El Deeb. Thermophoresis for characterizing biomolecular interaction. *Methods*, 146:107–119, 2018.

[12] D. Niether and S. Wiegand. Thermophoresis of biological and biocompatible compounds in aqueous solution. *J. Phys. Condes. Matter*, 31(50):503003, 2019.

[13] F. Tian, Z. Han, J. Deng, C. Liu, and J. Sun. Thermomicrofluidics for biosensing applications. *VIEW*, page 20200148, 2021.

[14] S. Mohanakumar, N. Lee, and S. Wiegand. Complementary Experimental Methods to Obtain Thermodynamic Parameters of Protein Ligand Systems. *Int. J. Mol. Sci.*, 23(22):14198, January 2022.

[15] T. J. Salez, B. T. Huang, M. Rietjens, M. Bonetti, C. Wiertel-Gasquet, M. Roger, C. L. Filomeno, E. Dubois, R. Perzynski, and S. Nakamae. Can charged colloidal particles increase the thermoelectric energy conversion efficiency? *Phys. Chem. Chem. Phys.*, 19:9409–9416, 2017.

[16] C.-G. Han, X. Qian, Q. Li, B. Deng, Y. Zhu, Z. Han, W. Zhang, W. Wang, S.-P. Feng, G. Chen, and W. Liu. Giant thermopower of ionic gelatin near room temperature. *Science*, 368(6495):1091–1098, 2020.

[17] Y. Jia, Q. Jiang, H. Sun, P. Liu, D. Hu, Y. Pei, W. Liu, X. Crispin, S. Fabiano, Y. Ma, and Y. Cao. Wearable thermoelectric materials and devices for self-powered electronic systems. *Adv. Mater.*, 33:e2102990, 2021.

[18] A. Parola and R. Piazza. Particle thermophoresis in liquids. *Eur. Phys. J. E*, 15:255–263, 2004.

[19] P. A. Artola, B. Rousseau, and G. Galliero. A new model for thermal diffusion: Kinetic approach. *J. Am. Chem. Soc.*, 130:10963–10969, 2008.

[20] A. Würger. Thermal non-equilibrium transport in colloids. *Rep. Prog. Phys.*, 73:126601, 2010.

[21] S. Di Lecce, T. Albrecht, and F. Bresme. The role of ion-water interactions in determining the soret coefficient of licl aqueous solutions. *Phys. Chem. Chem. Phys.*, 19:9575–9583, 2017.

[22] G. M. Whitesides. The origins and the future of microfluidics. *Nature*, 442(7101):368–373, 2006.

[23] N. Lee, S. Mohanakumar, and S. Wiegand. Thermophoretic microfluidic cells for evaluating Soret coefficient of colloidal particles. *Int. J. Heat Mass Trans.*, 194:123002, 2022.

[24] W.-Z. Fang, T. Xiong, O. S. Pak, and L. Zhu. Data-Driven Intelligent Manipulation of Particles in Microfluidics. *Adv. Sci.*, 10(5):2205382, 2023.

[25] S. R. de Groot and P. Mazur. *Non-equilibrium Thermodynamics*. Dover, New York, 1984.

[26] R. Rusconi, L. Isa, and R. Piazza. Thermal-lensing measurement of particle thermophoresis in aqueous dispersions. *J. Opt. Soc. Am. B*, 21:605–616, 2004.

[27] P. Polyakov and S. Wiegand. Investigation of the soret effect in aqueous and non-aqueous mixtures by the thermal lens technique. *Phys. Chem. Chem. Phys.*, 11:864–871, 2009.

[28] W. Köhler and P. Rossmanith. Aspects of thermal-diffusion forced rayleigh-scattering - heterodyne-detection, active phase tracking, and experimental constraints. *J. Phys. Chem.*, 99:5838–5847, 1995.

[29] S. Wiegand, H. Ning, and H. Kriegs. Thermal diffusion forced rayleigh scattering setup optimized for aqueous mixtures. *J. Phys. Chem. B*, 111(51):14169–14174, 2007.

[30] R. Piazza. Thermal diffusion in ionic micellar solutions. *Philos. Mag.*, 83:2067–2085, 2003.

[31] A. Königer, B. Meier, and W. Köhler. Measurement of the soret, diffusion, and thermal diffusion coefficients of three binary organic benchmark mixtures and of ethanol-water mixtures using a beam deflection technique. *Philos. Mag.*, 89:907–923, 2009.

[32] I. Dueramae, M. Yoneyama, N. Shinyashiki, S. Yagihara, and R. Kita. Thermal diffusion of aqueous solution of acetylated dextran: The effect of hydrophobicity using optical beam deflection technique. *Int. J. Heat Mass Transf.*, 132:997–1003, 2019.

[33] M. M. Bou-Ali, O. Ecenarro, J. A. Madariaga, C. M. Santamaria, and J. J. Valencia. Thermogravitational measurement of the soret coefficient of liquid mixtures. *J. Phys.: Condens. Matter*, 10(15):3321–3331, 1998.

[34] D. Vigolo, R. Rusconi, H. A. Stone, and R. Piazza. Thermophoresis: microfluidics characterization and separation. *Soft Matter*, 6(15):3489–3493, 2010.

[35] Y. Zhou, C. Yang, Y. C. Lam, and X. Huang. Thermophoresis of charged colloidal particles in aqueous media – effect of particle size. *Int. J. Heat Mass Transf.*, 101:1283–1291, 2016.

[36] T. Tsuji, K. Kozai, H. Ishino, and S. Kawano. Direct observations of thermophoresis in microfluidic systems. *Micro Nano Lett.*, 12(8):520–525, 2017.

[37] A. Errarte, A. Martin-Mayor, M. Aginagalde, I. Iloro, E. Gonzalez, J. M. Falcon-Perez, F. Elortza, and M. M. Bou-Ali. Thermophoresis as a technique for separation of nanoparticle species in microfluidic devices. *Int. J. Therm. Sci.*, 156:106435, October 2020.

[38] A. Sanjuan, A. Errarte, and M. M. Bou-Ali. Analysis of thermophoresis for separation of polystyrene microparticles in microfluidic devices. *Int. J. Heat Mass Transf.*, 189:122690, June 2022.

[39] L. Gong, A. Cretella, and Y. Lin. Microfluidic systems for particle capture and release: A review. *Biosens. Bioelectron.*, 236:115426, September 2023.

[40] S. Shakib, B. Rogez, S. Khadir, J. Polleux, A. Würger, and G. Baffou. Microscale Thermophoresis in Liquids Induced by Plasmonic Heating and Characterized by Phase and Fluorescence Microscopies. *J. Phys. Chem. C*, 125(39):21533–21542, 2021.

[41] H. Xu, X. Zheng, and X. Shi. Surface hydrophilicity-mediated migration of nano/microparticles under temperature gradient in a confined space. *J. Colloid Interf. Sci.*, 637:489–499, May 2023.

[42] N. Lee and S. Wiegand. Thermophoretic micron-scale devices: Practical approach and review. *Entropy*, 22(9):950, 2020.

[43] N. Lee, B.S. Kim, T. Kim, J.-Y. Bae, and H.H. Cho. Thermal design of helium cooled divertor for reliable operation. *Appl. Therm. Eng.*, 110:1578–1588, 2017.

[44] W. H. Reid and D. L. Harris. Some further results on the bénard problem. *Phys. Fluids*, 1(2):102, 1958.

[45] K. Clusius and G. Dickel. Das Trennrohr: I. Grundlagen eines neuen Verfahrens zur Gasentmischung und Isotopentrennung durch Thermodiffusion. *Z. Phys. Chem.*, 44B(1):397–450, 1939.

[46] O. Ecenarro, J. A. Madariaga, J. L. Navarro, C. M. Santamaria, J. A. Carrion, and J. M. Saviron. Thermogravitational Thermal-Diffusion in Liquid Polymer- Solutions. *Macromolecules*, 27(18):4968–4971, 1994.